CrossMark

INVITED ARTICLE

Liquid–liquid extraction of oxide particles and application in supercapacitors

Ri Chen
Department of Mechanical Engineering, McMaster University, Hamilton, Ontario, Canada L8S 4L7; and Department of Materials Science and Engineering, McMaster University, Hamilton, Ontario, Canada L8S 4L7

Mustafa S. Ata and Xinya Zhao
Department of Materials Science and Engineering, McMaster University, Hamilton, Ontario, Canada L8S 4L7

Ishwar Puri
Department of Mechanical Engineering, McMaster University, Hamilton, Ontario, Canada L8S 4L7; and Department of Materials Science and Engineering, McMaster University, Hamilton, Ontario, Canada L8S 4L7

Igor Zhitomirsky[a)]
Department of Materials Science and Engineering, McMaster University, Hamilton, Ontario, Canada L8S 4L7

(Received 8 December 2016; accepted 3 March 2017)

Many material manufacturing techniques require the use of nonaqueous colloidal suspensions, containing well dispersed oxide particles and various water insoluble functional components. We report an efficient method for the direct transfer of MnO_2 and titania particles, synthesized in water, to an organic solvent through the interface of two immiscible liquids. Particle agglomeration during the drying stage was avoided, and stable suspensions of nonagglomerated particles in the organic phase were obtained. The benefits of this method were demonstrated by the fabrication of advanced composite MnO_2-multiwalled carbon nanotube electrodes, containing a polymer binder, for electrochemical supercapacitors with high active mass loading and high active material to current collector mass ratio. The electrodes showed a capacitance of 5.13 F/cm^2 and low impedance. High extraction efficiency from concentrated suspensions was achieved by the use of an advanced extractor, which allowed strong adsorption on the particles by the polydentate bonding. The extraction mechanism is discussed.

I. INTRODUCTION

Particle extraction through liquid–liquid interface (PELLI) is emerging as a new method of technological and scientific interest. PELLI has been utilized for the separation of rare earth fluorescent powders,[1] alumina and zircon.[2] Size-dependent transfer of gold particles allowed obtaining suspensions with narrow particle size distribution.[3] PELLI has been utilized in the hydrometallurgy of cassiterite[4] and other mineral particles.[5] Luminescent CdTe and HgTe quantum dots, synthesized in an aqueous medium, were transferred to nonpolar organic solvents for the fabrication of photovoltaic and optoelectronic devices.[6]

Various organic molecules were used as extractors for PELLI applications. The chemical structures of such molecules contained hydrophobic hydrocarbon chains and functional groups, which provided electrostatic or chemical interactions with inorganic particles. Investigations were focused on the use of ionic surfactants,[1–5] which had an electric charge, opposite to that of inorganic particles. In this case, the surfactant adsorption was governed by electrostatic interactions with inorganic particles. Ion-pair interactions of carboxylate-modified gold nanoparticles and cationic surfactants resulted in the particle transfer from water to toluene.[7] The adsorption of other extractors, such as thiol based molecules and fatty acids, on inorganic particles involved chemical interactions. The molecules containing thiol groups allowed for partial extraction of CdTe and HgTe quantum dots.[6] The chemical interactions of carboxylic groups of fatty acids with iron atoms on the particle surface allowed for magnetite particle extraction.[8] Long chain surfactants, containing amino groups, were investigated for the extraction of gold[9–11] and silver[12] nanoparticles. It was found that polymer molecules can also be used as extractors.[13] The extraction efficiency was enhanced in the presence of co-solvents, such as sub-oil phase[5] or acetone.[6] In another strategy,[14] PELLI was triggered by changes of the temperature. The temperature increase from the room temperature to 80 °C resulted in the reduction of the solubility of the polymer extractor in an aqueous phase and transfer of the adsorbed particles to an organic phase.[14]

Contributing Editor: Eugene Medvedovski
[a)]Address all correspondence to this author.
e-mail: zhitom@mcmaster.ca
DOI: 10.1557/jmr.2017.92

 © Materials Research Society 2017

https://doi.org/10.1557/jmr.2017.92 Published online by Cambridge University Press

Previous PELLI research has been mainly focused on nanoparticles of metals and semiconductor quantum dots. The development of PELLI methods for oxide nanoparticles offers benefits for many applications. Various applications of oxide materials in thin film electronic devices, protective coatings, sensors, biomedical implants, aqueous batteries, and supercapacitors require the use of water insoluble organic components, such as binders, film forming agents, and functional organic molecules.[15,16] In many manufacturing procedures, oxide nanoparticles must be dispersed in an organic solvent, containing dissolved functional organic molecules or macromolecules, which are insoluble in water. It is important to note that many important techniques for the oxide nanoparticle synthesis are based on aqueous processing. The synthesized nanoparticles are usually dried and then redispersed in an organic solvent. However, the drying of the oxide or hydroxide particles results in their agglomeration. The reduction of particle surface area and condensation of surface OH groups are major driving forces for particle agglomeration. The important task is the development of PELLI methods for the transfer of synthesized oxide nanoparticles directly from an aqueous phase to an organic phase, avoiding the drying procedure. However, poor adsorption of extractor molecules on oxide particles and low extraction efficiency are still major obstacles in achieving this goal.

The selection of extractor molecules with strong adsorption on the particle surface is of critical importance for the development of PELLI methods. The approach, based on the electrostatic interaction of surfactants and particles, has limitations related to the control of particle charge in water as well as in organic phases and low recovery efficiency, attributed to weak surfactant adsorption on particles. The extractor molecules, containing carboxylate, amino, and thiol groups, allow for relatively weak bonding and poor adsorption on the oxide particles.

The goal of this investigation was the development of an efficient PELLI method for oxide particles. The approach is based on the use of hexadecylphosphonic acid (HDPA) as an advanced extractor molecule. The chemical structure of HDPA [Fig. 1(A)] contains a phosphonate group. Literature data indicate that phosphonates exhibit strong adsorption in water on various inorganic materials,[17–23] such as hydroxyapatite, Fe_3O_4, SiO_2, ZnO, Al_2O_3, TiO_2, clay, calcium carbonate, and indium tin oxide. The oxygen atoms of the phosphonate ligand allow for bi- or tridentate bonding [Fig. 1(B)], which results in significantly stronger adsorption, compared to monodentate bonding[24] of many extractor and dispersant molecules. The chelation bonding {Fig. 1[B(a,b)]} involves the formation of the coordination bonds between two or three oxygen atoms of HDPA and a metal atom on the particle surface. The oxygen atoms of the phosphonate ligand can also be bonded to different metal atoms {Fig. 1[B(c,d)]}.

We report the synthesis of MnO_2 and titania particles in aqueous solutions and their extraction to the *n*-butanol phase [Fig. 1(C)], containing dissolved HDPA. In this strategy, water insoluble HDPA molecules adsorbed on oxide particles at the water-*n*-butanol interface. The results presented below indicated high extraction efficiency and reduced particle agglomeration. An important outcome of this study was the fabrication of MnO_2-multiwalled carbon nanotube (MWCNT) composites for application in electrodes of electrochemical supercapacitors, which showed promising capacitive properties.

II. EXPERIMENTAL PROCEDURES

HDPA, poly(vinyl butyral-co-vinyl alcohol-co-vinyl acetate) (PVB, average M_w = 50,000–80,000), $NaMnO_4$, $TiOSO_4$, NaOH, Na_2SO_4, *n*-butanol (Aldrich, Oakville, Canada), and MWCNTs (ID 4 nm, OD 13 nm, length 1–2 μm, Bayer, Leverkusen, Germany) were used. Ni foams with 95% porosity were provided by Vale Company (Mississauga, Canada).

The synthesis of MnO_2 particles was performed by a chemical precipitation method using aqueous $NaMnO_4$ solutions and *n*-butanol as a reducing agent. Previous investigations[25–27] showed that various alcohols, such as ethanol, isopropanol, methanol, and other alcohols, miscible with water, can be used as reducing agents for the synthesis of MnO_2 from permanganate solutions. In this investigation, water-immiscible *n*-butanol was used as a reducing agent for $NaMnO_4$. The addition of *n*-butanol to aqueous solutions and stirring for 1 h resulted in the precipitation of MnO_2 in an aqueous phase [Figs. 2(a) and 2(b)]. Further addition of HDPA solution in *n*-butanol and stirring resulted in the extraction of MnO_2 from the aqueous phase to *n*-butanol phase [Fig. 2(c)]. The MnO_2 particles formed a stable suspension in the *n*-butanol phase. The synthesis of titania was performed using aqueous $TiOSO_4$ solutions. The pH of the solutions was adjusted to pH = 6 by NaOH. The addition of HDPA solution in *n*-butanol and stirring resulted in the extraction of titania from the aqueous phase to *n*-butanol phase [Figs. 2(d) and 2(e)]. The extracted titania formed a stable suspension in *n*-butanol. The mass of extracted MnO_2 or titania particles was varied in the range of 0.3–1.0 g. The mass ratio of HDPA:oxide was 0.2–0.3.

Electron microscopy investigations were performed using a JEOL JSM-7000F scanning electron microscope (SEM; JEOL Ltd., Tokyo, Japan). X-ray diffraction (XRD) studies were performed using a powder diffractometer (Nicolet I2, Nicolet, San Diego, California; monochromatized Cu K_α radiation). The materials for the XRD and SEM studies were prepared using suspensions, as shown in Figs. 2(b) and 2(d). The suspensions were filtrated, washed with water and ethanol, and then dried in air for 72 h. Fourier transform infrared spectroscopy (FTIR) studies were performed on

https://doi.org/10.1557/jmr.2017.92 Published online by Cambridge University Press

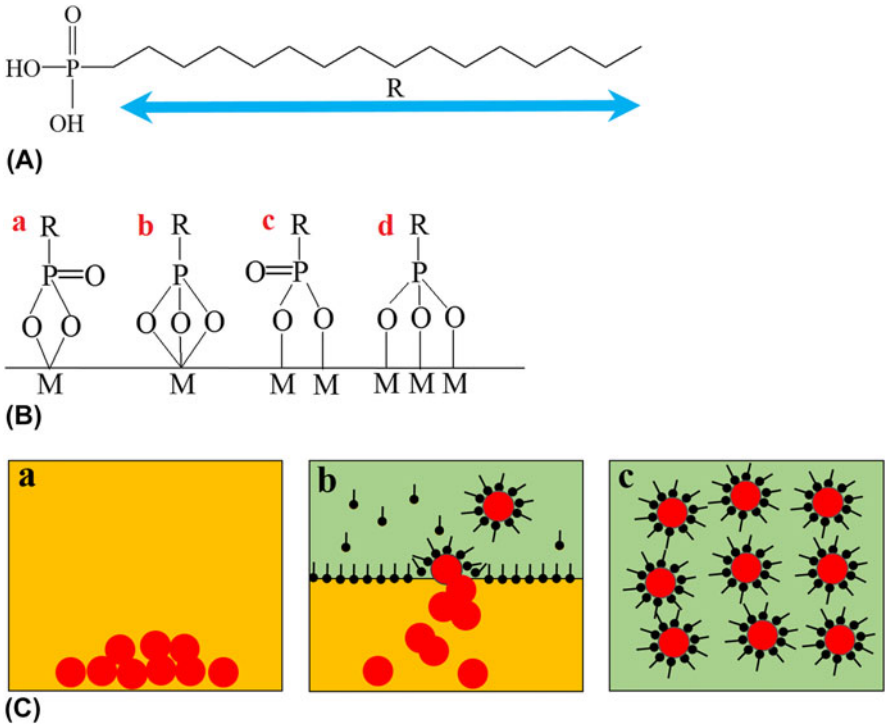


FIG. 1. (A) Chemical structure of HDPA (B) adsorption mechanisms of HDPA, involving (a) chelating bidentate bonding, (b) chelating tridentate bonding, (c) bridging bidentate bonding, (d) bridging tridentate bonding, (C) schematic of the PELLI method: (a) particles, precipitated in aqueous phase, (b) transfer through liquid–liquid interface, (c) formation of a stable suspension of particles in *n*-butanol.

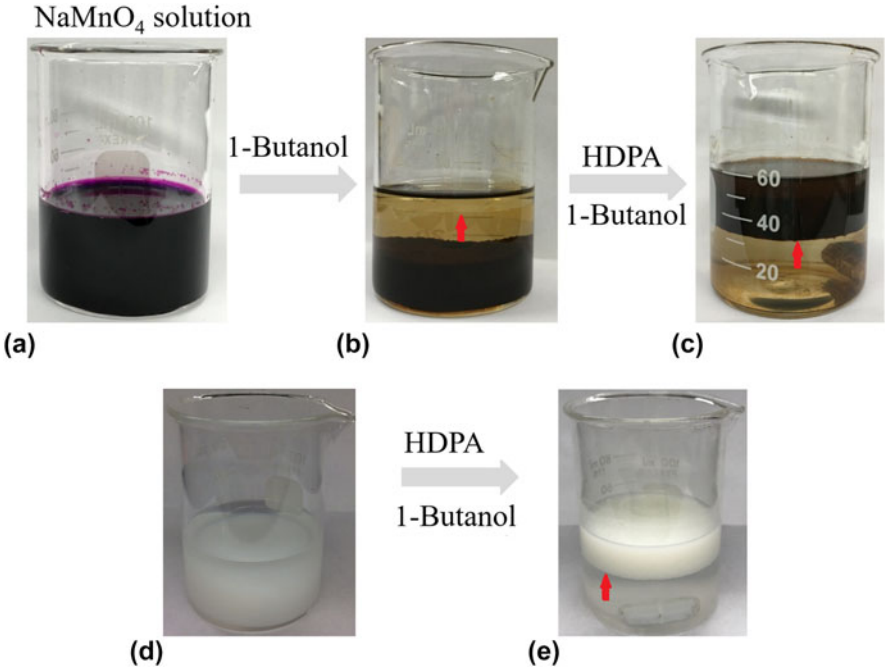


FIG. 2. (a) $NaMnO_4$ solution, (b) precipitation of MnO_2 after mixing of $NaMnO_4$ with *n*-butanol, (c) extraction of MnO_2 to the *n*-butanol solvent after addition of HDPA solution in *n*-butanol and mixing, (d) as-precipitated titania in water, (e) extraction of titania to the *n*-butanol solvent after addition of HDPA solution in *n*-butanol and mixing, red arrows show the interface of water and *n*-butanol.

a Bruker Vertex 70 spectrometer (Bruker, Milton, Canada). For the preparation of samples for the FTIR studies, the suspensions, shown in Figs. 2(c) and 2(e), were filtrated and the obtained materials were dried in air. Dynamic light scattering (DLS, DelsaMax Pro: Beckman Coulter, Brea, California) was used for the particle size distribution

https://doi.org/10.1557/jmr.2017.92 Published online by Cambridge University Press

analysis. The suspensions of particles in *n*-butanol, separated from the aqueous phase, were diluted with ethanol for the particle distribution analysis.

The suspension of MWCNT in *n*-butanol was added to MnO_2 suspension to obtain the MnO_2:MWCNT mass ratio of 4:1. The organic suspension was separated from the aqueous phase, ultrasonicated, and then the solution of PVB binder in ethanol was added. Obtained suspension was used for the fabrication of MnO_2-MWCNT electrodes by impregnation of the Ni foam current collectors. The active mass loading of the electrodes was 35.5 mg/cm^2.

Cyclic voltammetry (CV) and impedance spectroscopy investigations were performed using a potentiostat (PARSTAT 2273; Princeton Applied Research, Oak Ridge, Tennessee). Capacitive behavior of the electrodes was studied in three-electrode cells using 0.5 M Na_2SO_4 aqueous solutions. The area of the working electrode was 1 cm^2. The counter electrode was a platinum gauze, and the reference electrode was a standard calomel electrode (SCE). CV studies were performed at scan rates of 2–100 mV/s. The integral capacitances $C_s = Q/\Delta VS$ and $C_m = Q/\Delta Vm$ were calculated using half the integrated area of the CV curve to obtain the charge Q, and subsequently dividing the charge Q by the width of the potential window ΔV and electrode area S or active mass m. The alternating current measurements of complex impedance $Z^* = Z' - iZ''$ were performed in the frequency range of 10 mHz–100 kHz at the amplitude of the signal of 5 mV. The complex differential capacitance $C_s^* = C_s' - iC_s''$ was calculated[28] from the impedance data as $C_s' = Z''/\omega|Z|^2S$ and $C_s'' = Z'/\omega|Z|^2S$, where $\omega = 2\pi f$ (f-frequency).

III. RESULTS AND DISCUSSION

The successful extraction of MnO_2 and titania from water to *n*-butanol was achieved using HDPA as an advanced extractor. The polydentate bonding of the phosphonate groups of HDPA to the metal atoms on the particle surface allowed for strong adsorption, which was confirmed in several experiments, discussed below. After synthesis, the MnO_2 particles accumulated in the aqueous phase [Fig. 2(b)] and precipitated. Figure 2(b) shows a clear supernatant *n*-butanol solvent without MnO_2 particles. However, the addition of HDPA solution to *n*-butanol allowed for the bottom–up extraction of MnO_2 particles from the bottom aqueous phase to the top organic phase against the force of gravity [Fig. 2(c)]. The titania particles showed a similar behavior (Fig. 2(e)]. Our approach is different from the top–down strategy,[29] where the gravitational force promoted the transfer of destabilized agglomerated particles from water to an organic liquid with higher density. The colloidal stabilization of the particles in the *n*-butanol solvent indicated that adsorbed HDPA provided a steric stabilization. The extracted particles have also been analyzed by the FTIR method. Figure 3 compares the FTIR spectra of the extracted particles and HDPA. The absorptions in the range of 2800–3000 cm^{-1} in the spectra of MnO_2 and titania particles are attributed to stretching vibrations[30,31] of CH_2 and CH_3 groups of adsorbed HDPA. The FTIR spectrum of pure HDPA showed similar absorptions. The adsorptions at 1469 cm^{-1} in the spectra of particles and corresponding adsorption at 1471 cm^{-1} in the spectrum of pure HDPA resulted from the deformation C–H vibrations[30] of HDPA. The strong adsorption of HDPA was critical for the extraction. The insolubility of HDPA in water is another important factor, which was considered for the selection of this molecule as an extractor.

The extraction mechanism involved the adsorption of HDPA on the particles at the interface of the two immiscible liquids and transfer of the inorganic particles to the *n*-butanol phase by the adsorbed HDPA. In our investigation, *n*-butanol was used as a reducing agent for the synthesis of MnO_2 and as a receiving liquid in the PELLI method. However, the influence of the nature of the receiving liquid and liquid–liquid interface on the extraction process is not well understood. It should be noted that the adsorption of organic molecules on the particle surface is influenced by a solvent.[32,33] Other observations indicated that the modification of water-oil mixtures by the sub-oil phases was beneficial for the particle transfer through the interface.[5] It is known that the surfactant concentration increases at the liquid–liquid interface.[29] From this point of view, the accumulation of HDPA at the interface was beneficial for interaction with particles and their extraction. In many investigations, the liquid–liquid interface was used as a platform for the 2D assembly of particles.[34,35] It was found that the driving force for particle accumulation at the interface is the reduction of the interface surface energy between two liquids.[34,36] However, in our experiments, MnO_2

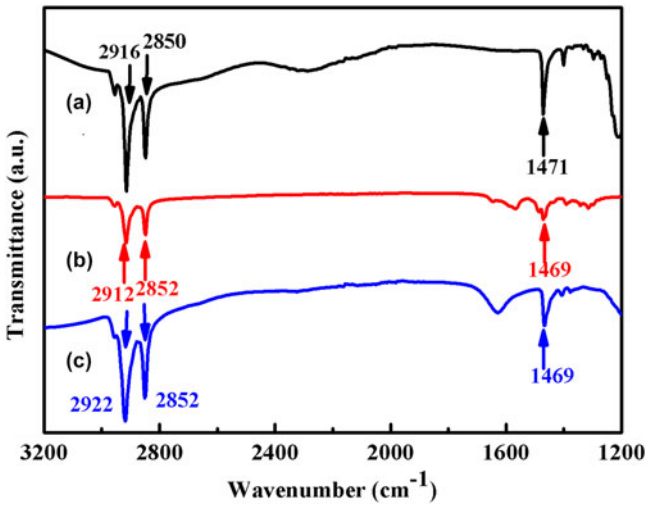


FIG. 3. FTIR spectra of (a) HDPA and of extracted materials: (b) MnO_2 and (c) titania.

https://doi.org/10.1557/jmr.2017.92 Published online by Cambridge University Press

particles precipitated in the aqueous phase [Fig. 2(b)]. The stirring and ultrasonication promoted their transfer to the liquid–liquid interface, where HDPA molecules adsorbed on the particles. It is known that the adsorption of surfactant molecules on the particle surface at the liquid–liquid interface[34] can result in reduced interfacial energy. It is in this regard that the liquid–liquid interface provides unique conditions, which facilitate various chemical reactions.[34,36,37] The modification of particles at the liquid–liquid interface with adsorbed HDPA promoted particle transfer from water to *n*-butanol in the PELLI method.

It is important to note that many PELLI applications were limited to the use of relatively dilute suspensions.[3,10,12] In our investigation, the application of HDPA as an advanced extractor allowed the use of suspensions of significantly higher concentrations. The typical particle concentration in the *n*-butanol phase was 15–50 g/L. The experimental results presented below indicated that concentrated suspensions are beneficial for practical applications for the fabrication of supercapacitor electrodes by impregnation of current collectors with an active material.

The MnO_2 and titania particles, synthesized in aqueous phases, showed poor colloidal stability and precipitated immediately after stirring or ultrasonic agitation. In contrast, the extracted particles showed a good colloidal stability in the *n*-butanol phase. The good dispersion of particles and suspension stability are critical for colloidal processing of oxide materials and composites.[38]

The suspensions, shown in Figs. 2(b) and 2(d), were filtrated, washed in water, dried in air for 72 h, and studied by XRD and SEM. The XRD patterns (Fig. 4) showed that MnO_2 and titania were mainly amorphous. However, small broad peaks of the birnessite phase were observed in the XRD pattern of MnO_2. The peak broadening resulted from the small particle size. The formation of mainly amorphous MnO_2, containing a small amount of a birnessite phase, was also observed in other investigations, where $KMnO_4$ was reduced with different alcohols, such as ethanol[39] or isopropanol.[40] The SEM studies [Fig. 5(a)] showed that the MnO_2 powder contained relatively small particles with a typical size of 0.1 μm and agglomerates. The size of the agglomerates was in the range of 0.2–5 μm. The SEM images of the titania powder [Fig. 5(b)] showed relatively large agglomerates with a typical size of 2–20 μm. In contrast, the investigation of extracted particles by the DLS method showed that the average radius of MnO_2 and titania particles was 90.6 and 188.1 nm, respectively (Fig. 6). The extracted particles showed relatively small polydispersity indexes of 11.3 and 11.7% for MnO_2 and titania, respectively. The small polydispersity indexes indicated a high level homogeneity of the sizes of the particles. Multiple testing experiments showed well repeatable results due to the use of stable suspensions. In contrast, the redispersion of dried powders, shown in Fig. 5 in ethanol, resulted in unstable suspensions. The analysis of particles in such suspensions by the DLS method presented difficulties due to rapid sedimentation of the particles. The sedimentation resulted in significant variations of the measured average particle size and time dependent polydispersity indexes. The typical polydispersity indexes were above 45%.

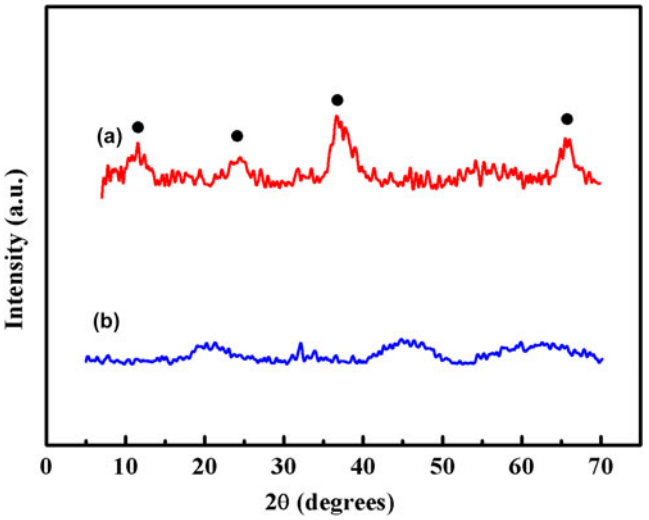


FIG. 4. XRD patterns of (a) MnO_2 (•—JCPDS file 87–1497) and (b) titania.

The ability to transfer MnO_2 and titania particles, synthesized in water, to an organic solvent and avoid particle agglomeration during the drying stage offers benefits for many applications, utilizing advanced properties of such materials. Of particular importance is the application of the PELLI method for the fabrication of advanced electrodes for electrochemical supercapacitors. As a step in this direction, we investigated MnO_2 particles, prepared using the PELLI method.

The charge storage properties of MnO_2 are related to the redox reaction[41]

$$MnO_2 + A^+ + e^- \leftrightarrow MnO_2A \quad , \qquad (1)$$

where $A^+ = Na^+, K^+, H^+$. The use of MnO_2 as a charge storage material offers the advantages[41–43] of high theoretical specific capacitance (1370 F/g) and nearly ideal capacitive behavior in a voltage window of ~0.9 V in mild aqueous electrolytes, such as K_2SO_4 or Na_2SO_4. Eq. (1) indicates that high electronic and ionic conductivities of the electrode material are important for the efficient charge–discharge behavior. Conductive additives, such as MWCNT, are usually added to MnO_2 to improve the electronic conductivity. However, the specific capacitance of MWCNT is low. Therefore, the amount of MWCNT in the composite electrode must be

https://doi.org/10.1557/jmr.2017.92 Published online by Cambridge University Press

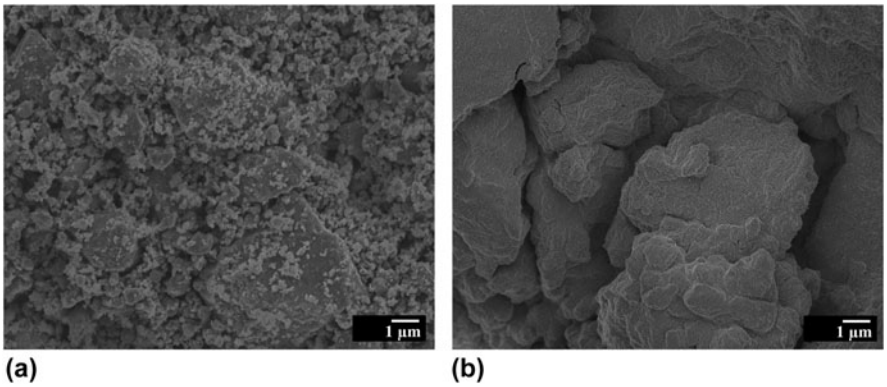


FIG. 5. SEM images of (a) MnO_2 and (b) titania, prepared from suspensions, shown in Figs. 2(b) and 2(d), respectively, after filtration, washing with water, and drying in air for 72 h.

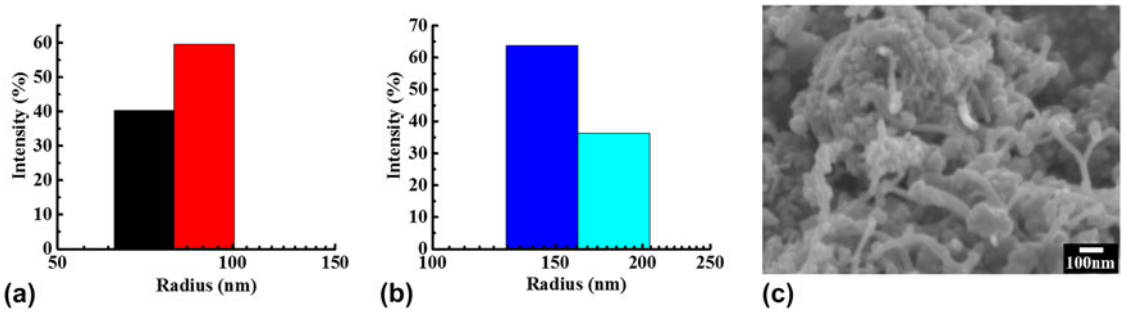


FIG. 6. Particle size distributions for (a) MnO_2 and (b) titania, extracted using HDPA and (c) SEM image of MnO_2-MWCNT composite.

optimized. An important task is to avoid MnO_2 particle agglomeration and achieve good electrolyte access to the active material. Good dispersion and mixing of non-agglomerated MnO_2 and MWCNT are extremely important for the electrode performance. The ability to achieve high capacitance at high active mass loadings is one of the challenges in the supercapacitor technology. Literature data indicate that the gravimetric capacitance decreased by one order of magnitude with an increase of electrode mass due to poor utilization of the capacitive properties of MnO_2.[44–47] Another important parameter is the ratio of active material mass to the current collector mass (R_m). Relatively high specific capacitances were achieved in thin films with an active mass of 0.005–2 mg/cm^2, deposited on foil substrates.[45–48] However, R_m for such films is only 5×10^{-5} to 5×10^{-2}. A relatively small areal capacitance can be achieved at such small mass loadings.

The extracted MnO_2 formed stable concentrated suspensions, suitable for the impregnation of Ni foam current collectors and fabrication of the supercapacitor electrodes. MWCNT was added to the suspensions with mass ratio of MnO_2:MWCNT = 4:1. The PVB binder was added in order to achieve 3% mass content of PVB in the composite electrode. The suspension was impregnated into the Ni foam. The total mass of the impregnated material after drying was 35.5 mg/cm^2 and R_m was 0.5. The SEM image of the MnO_2-MWCNT composite [Fig. 6(c)] shows a good dispersion of MWCNT in the MnO_2 matrix.

Figure 7(A) shows CVs at different scan rates for the composite MnO_2-MWCNT electrodes. The nearly ideal box shape CVs and increase of current with increasing scan rate indicated good capacitive behavior. The electrodes showed a relatively high gravimetric capacitance [Fig. 7(B)] at high active mass loading (35.5 mg/cm^2), which was comparable with the capacitance, achieved in the literature at small mass loadings (0.1–2 mg/cm^2).[46,47,49] The highest capacitance C_m of 144.5 F/g was obtained at a scan rate of 2 mV/s. However, due to the use of high active material loading, we were able to achieve a high areal capacitance C_s of 5.13 F/cm^2 at a scan rate of 2 mV/s. At high scan rates, we observed a significant improvement in capacitance retention, compared to the electrodes, prepared using advanced co-dispersants for MnO_2 and MWCNT.[50] The use of the PELLI method allowed ~2 times higher C_s at 50 and 100 mV/s, compared to C_s achieved at the same scan rates at a higher mass loading[50] of 40 mg/cm^2. The analysis of the impedance data [Fig. 8(a)] revealed a good capacitive behavior, as indicated by nearly 90° slope of the Nyquist plot. The electrodes offered an advantage of low resistance $R = Z'$. The low Z'' values resulted from high capacitance. The frequency dependences of the components of complex capacitance,

https://doi.org/10.1557/jmr.2017.92 Published online by Cambridge University Press

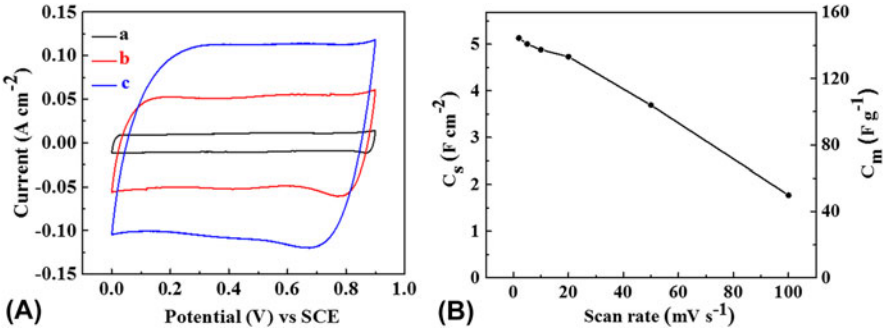


FIG. 7. (A) CVs at scan rates of (a) 2, (b) 10, and (c) 20 mV/s, (B) C_s and C_m, calculated from the CV data at different scan rates.

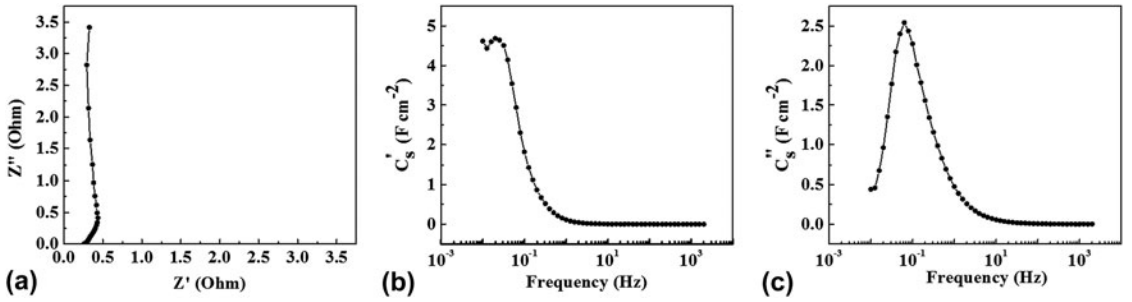


FIG. 8. (a) Nyquist plot for complex impedance and frequency dependences of (b) C_s' and (c) C_s'' calculated from the impedance data for MnO_2-MWCNT electrodes.

calculated from the impedance data, are presented in Figs. 8(b) and 8(c). The real component of the differential capacitance C_s' at low frequencies was slightly lower than the integral capacitance C_s at low scan rates. It should be noted that the differential capacitance was measured at significantly lower voltages (5 mV). It was mentioned in the previous investigation[51] that lower differential capacitance can result from limited electrolyte access to some active sites of the capacitive material at low voltages. It is important to note that integral capacitance depends of scan rate, whereas the differential capacitance is a function of frequency. The frequency dependences of the components of differential capacitance showed a relaxation type dispersion, as indicated by the reduction of C_s' with frequency and a maximum in the frequency dependence of C_s''. The relatively high relaxation frequency, corresponding to the C_s'' maximum, indicates a good capacitive behavior at high charge–discharge rates.

IV. CONCLUSIONS

A new PELLI method has been developed for the fabrication of stable MnO_2 and titania suspensions in *n*-butanol. High extraction efficiency was achieved from concentrated suspensions using HDPA as an advanced extractor. The important factors for the efficient extraction are water insolubility of HDPA and its strong adsorption on the inorganic nanoparticles, involving the polydentate bonding. The extraction mechanism was based on the interaction of HDPA and the inorganic particles at the liquid–liquid interface. The problems, related to the particle agglomeration during the drying stage, were avoided in the PELLI method. The ability to transfer synthesized particles from water to the organic solvent and obtain concentrated and stable suspensions allowed for the impregnation of Ni foam current collectors using slurries of MnO_2 and MWCNT, containing a solution of water insoluble PVB binder. The reduced agglomeration and efficient mixing of MnO_2 and MWCNT allowed for the fabrication of advanced electrodes with high active mass loading and high active material to current collector mass ratio, which showed good capacitive performance and low impedance. The capacitance of 5.13 F/cm^2 was achieved at a scan rate of 2 mV/s. The electrodes, prepared by the PELLI method, are promising for energy storage in electrochemical supercapacitors. The PELLI method can be used for other applications, which require agglomerate-free colloidal processing of oxide materials and composites.

ACKNOWLEDGMENTS

The authors gratefully acknowledge the Natural Sciences and Engineering Research Council of Canada for the financial support and Vale Canada for the donation of Ni foam.

https://doi.org/10.1557/jmr.2017.92 Published online by Cambridge University Press

REFERENCES

1. A. Otsuki, G. Dodbiba, A. Shibayama, J. Sadaki, G. Mei, and T. Fujita: Separation of rare earth fluorescent powders by two-liquid flotation using organic solvents. *Jpn. J. Appl. Phys.* **47**, 5093 (2008).
2. L.P. Wang, Y. Kanemitsu, G. Dodbiba, T. Fujita, Y. Oya, and H. Yokoyama: Separation of ultrafine particles of alumina and zircon by liquid–liquid extraction using kerosene as the organic phase and sodium dodecylsulfate (SDS) as the surfactant collector for abrasive manufacturing waste recycling. *Sep. Purif. Technol.* **108**, 133 (2013).
3. W. Cheng and E. Wang: Size-dependent phase transfer of gold nanoparticles from water into toluene by tetraoctylammonium cations: A wholly electrostatic interaction. *J. Phys. Chem. B* **108**, 24 (2004).
4. G. Zambrana, R. Medina, G. Gutierrez, and R. Vargas: Recovery of minus ten micron cassiterite by liquid–liquid extraction. *Int. J. Miner. Process.* **1**, 335 (1974).
5. B. Hu, Y. Nakahiro, and T. Wakamatsu: The effect of organic solvents on the recovery of fine mineral particles by liquid–liquid extraction. *Miner. Eng.* **6**, 731 (1993).
6. N. Gaponik, D.V. Talapin, A.L. Rogach, A. Eychmuller, and H. Weller: Efficient phase transfer of luminescent thiol-capped nanocrystals: From water to nonpolar organic solvents. *Nano Lett.* **2**, 803 (2002).
7. H. Yao, O. Momozawa, T. Hamatani, and K. Kimura: Phase transfer of gold nanoparticles across a water/oil interface by Stoichiometric ion-pair formation on particle surfaces. *Bull. Chem. Soc. Jpn.* **73**, 2675 (2000).
8. J. Erler, S. Machunsky, P. Grimm, H-J. Schmid, and U.A. Peuker: Liquid–liquid phase transfer of magnetite nanoparticles-evaluation of surfactants. *Powder Technol.* **247**, 265 (2013).
9. M. Karg, N. Schelero, C. Oppel, M. Gradzielski, T. Hellweg, and R. von Klitzing: Versatile phase transfer of gold nanoparticles from aqueous media to different organic media. *Chem.–Eur. J.* **17**, 4648 (2011).
10. A. Kumar, P. Mukherjee, A. Guha, S. Adyantaya, A. Mandale, R. Kumar, and M. Sastry: Amphoterization of colloidal gold particles by capping with valine molecules and their phase transfer from water to toluene by electrostatic coordination with fatty amine molecules. *Langmuir* **16**, 9775 (2000).
11. K.S. Mayya and F. Caruso: Phase transfer of surface-modified gold nanoparticles by hydrophobization with alkylamines. *Langmuir* **19**, 6987 (2003).
12. A. Kumar, H. Joshi, R. Pasricha, A. Mandale, and M. Sastry: Phase transfer of silver nanoparticles from aqueous to organic solutions using fatty amine molecules. *J. Colloid Interface Sci.* **264**, 396 (2003).
13. S. Underwood and P. Mulvaney: Effect of the solution refractive index on the color of gold colloids. *Langmuir* **10**, 3427 (1994).
14. X. Feng, H. Ma, S. Huang, W. Pan, X. Zhang, F. Tian, C. Gao, Y. Cheng, and J. Luo: Aqueous-organic phase-transfer of highly stable gold, silver, and platinum nanoparticles and new route for fabrication of gold nanofilms at the oil/water interface and on solid supports. *J. Phys. Chem. B* **110**, 12311 (2006).
15. T. Casagrande, G. Lawson, H. Li, J. Wei, A. Adronov, and I. Zhitomirsky: Electrodeposition of composite materials containing functionalized carbon nanotubes. *Mater. Chem. Phys.* **111**, 42 (2008).
16. Y. Su and I. Zhitomirsky: Hybrid MnO_2/carbon nanotube-VN/carbon nanotube supercapacitors. *J. Power Sources* **267**, 235 (2014).
17. S.P. Pujari, L. Scheres, A. Marcelis, and H. Zuilhof: Covalent surface modification of oxide surfaces. *Angew. Chem., Int. Ed.* **53**, 6322 (2014).
18. R. Boissezon, J. Muller, V. Beaugeard, S. Monge, and J-J. Robin: Organophosphonates as anchoring agents onto metal oxide-based materials: Synthesis and applications. *RSC Adv.* **4**, 35690 (2014).
19. B. Kalska-Szostko, M. Rogowska, and D. Satula: Organophosphorous functionalization of magnetite nanoparticles. *Colloids Surf., B* **111**, 656 (2013).
20. F. Li, H. Zhong, G. Zhao, S. Wang, and G. Liu: Adsorption of α-hydroxyoctyl phosphonic acid to ilmenite/water interface and its application in flotation. *Colloids Surf., A* **490**, 67 (2016).
21. C.l.S. Pauly, A-C. Genix, J.G. Alauzun, M. Sztucki, J. Oberdisse, and P.H. Mutin: Surface modification of alumina-coated silica nanoparticles in aqueous sols with phosphonic acids and impact on nanoparticle interactions. *Phys. Chem. Chem. Phys.* **17**, 19173 (2015).
22. G. Thomas, F. Demoisson, J. Boudon, and N. Millot: Efficient functionalization of magnetite nanoparticles with phosphonate using a one-step continuous hydrothermal process. *Dalton Trans.* **45**, 10821 (2016).
23. P. Kar, A. Pandey, J.J. Greer, and K. Shankar: Ultrahigh sensitivity assays for human cardiac troponin I using TiO_2 nanotube arrays. *Lab Chip* **12**, 821 (2012).
24. M. Ata, Y. Liu, and I. Zhitomirsky: A review of new methods of surface chemical modification, dispersion and electrophoretic deposition of metal oxide particles. *RSC Adv.* **4**, 22716 (2014).
25. V. Subramanian, H. Zhu, and B. Wei: Alcohol-assisted room temperature synthesis of different nanostructured manganese oxides and their pseudocapacitance properties in neutral electrolyte. *Chem. Phys. Lett.* **453**, 242 (2008).
26. M. Cheong and I. Zhitomirsky: Electrophoretic deposition of manganese oxide films. *Surf. Eng.* **25**, 346 (2009).
27. J. Li and I. Zhitomirsky: Electrophoretic deposition of manganese oxide nanofibers. *Mater. Chem. Phys.* **112**, 525 (2008).
28. P. Taberna, P. Simon, and J.F. Fauvarque: Electrochemical characteristics and impedance spectroscopy studies of carbon-carbon supercapacitors. *J. Electrochem. Soc.* **150**, A292 (2003).
29. S. Machunsky and U.A. Peuker: Liquid–liquid interfacial transport of nanoparticles. *Phys. Separ. Sci. Eng.* **2007**, 34832 (2007).
30. M. Giza, P. Thissen, and G. Grundmeier: Adsorption kinetics of organophosphonic acids on plasma-modified oxide-covered aluminum surfaces. *Langmuir* **24**, 8688 (2008).
31. E.S. Dzunuzovic, J.V. Dzunuzovic, A.D. Marinkovic, M.T. Marinovic-Cincovic, K.B. Jeremic, and J.M. Nedeljkovic: Influence of surface modified TiO_2 nanoparticles by gallates on the properties of PMMA/TiO_2 nanocomposites. *Eur. Polym. J.* **48**, 1385 (2012).
32. I. Zhitomirsky and A. Petric: Electrophoretic deposition of ceramic materials for fuel cell applications. *J. Eur. Ceram. Soc.* **20**, 2055 (2000).
33. I. Zhitomirsky and A. Petric: Electrophoretic deposition of electrolyte materials for solid oxide fuel cells. *J. Mater. Sci.* **39**, 825 (2004).
34. A. Toor, T. Feng, and T.P. Russell: Self-assembly of nanomaterials at fluid interfaces. *Eur. Phys. J. E* **39**, 1 (2016).
35. D.M. Andala, S.H.R. Shin, H-Y. Lee, and K.J. Bishop: Templated synthesis of amphiphilic nanoparticles at the liquid–liquid interface. *ACS Nano* **6**, 1044 (2012).
36. W.P. Lee, H. Chen, R. Dryfe, and Y. Ding: Kinetics of nanoparticle synthesis by liquid–liquid interfacial reaction. *Colloids Surfaces A.* **343**, 3 (2009).
37. X. Liang, L. Xing, J. Xiang, F. Zhang, J. Jiao, L. Cui, B. Song, S. Chen, C. Zhao, and H. Sai: The role of the liquid–liquid interface in the synthesis of nonequilibrium crystalline Wurtzite ZnS at room temperature. *Cryst. Growth Des.* **12**, 1173 (2012).
38. Y. Li, K. Wu, and I. Zhitomirsky: Electrodeposition of composite zinc oxide-chitosan films. *Colloids Surf., A* **356**, 63 (2010).

https://doi.org/10.1557/jmr.2017.92 Published online by Cambridge University Press

39. J. Li and I. Zhitomirsky: Cathodic electrophoretic deposition of manganese dioxide films. *Colloids Surf., A* **348**, 248 (2009).
40. G.M. Jacob, Q.M. Yang, and I. Zhitomirsky: Electrodes for electrochemical supercapacitors. *Mater. Manuf. Process.* **24**, 1359 (2009).
41. S. Devaraj and N. Munichandraiah: High capacitance of electrodeposited MnO_2 by the effect of a surface-active agent. *Electrochem. Solid-State Lett.* **8**, A373 (2005).
42. L. Athouel, F. Moser, R. Dugas, O. Crosnier, D. Bélanger, and T. Brousse: Variation of the MnO_2 birnessite structure upon charge/discharge in an electrochemical supercapacitor electrode in aqueous Na_2SO_4 electrolyte. *J. Phys. Chem. C* **112**, 7270 (2008).
43. D. Bélanger, T. Brousse, and J.W. Long: Manganese oxides: Battery materials make the leap to electrochemical capacitors. *Electrochem. Soc. Interf.* **17**, 49 (2008).
44. R. Jiang, T. Huang, Y. Tang, J. Liu, L. Xue, J. Zhuang, and A. Yu: Factors influencing MnO_2/multi-walled carbon nanotubes composite's electrochemical performance as supercapacitor electrode. *Electrochim. Acta* **54**, 7173 (2009).
45. M. Toupin, T. Brousse, and D. Belanger: Charge storage mechanism of MnO_2 electrode used in aqueous electrochemical capacitor. *Chem. Mater.* **16**, 3184 (2004).
46. K-W. Nam and K-B. Kim: Manganese oxide film electrodes prepared by electrostatic spray deposition for electrochemical capacitors. *J. Electrochem. Soc.* **153**, A81 (2006).
47. H. Xia and C. Huo: Electrochemical properties of MnO_2/CNT nanocomposite in neutral aqueous electrolyte as cathode material for asymmetric supercapacitors. *Int. J. Smart Nano Mater.* **2**, 283 (2011).
48. G.M. Jacob and I. Zhitomirsky: Microstructure and properties of manganese dioxide films prepared by electrodeposition. *Appl. Surf. Sci.* **254**, 6671 (2008).
49. J. Li and I. Zhitomirsky: Electrophoretic deposition of manganese dioxide-carbon nanotube composites. *J. Mater. Process. Technol.* **209**, 3452 (2009).
50. Y. Wang, Y. Liu, and I. Zhitomirsky: Surface modification of MnO_2 and carbon nanotubes using organic dyes for nanotechnology of electrochemical supercapacitors. *J. Mater. Chem. A* **1**, 12519 (2013).
51. Y. Zhu, K. Shi, and I. Zhitomirsky: Anionic dopant-dispersants for synthesis of polypyrrole coated carbon nanotubes and fabrication of supercapacitor electrodes with high active mass loading. *J. Mater. Chem. A* **2**, 14666 (2014).

https://doi.org/10.1557/jmr.2017.92 Published online by Cambridge University Press